PAPER

CrossMark
click for updates

Towards biolubricant compatible vegetable oils by pore mouth hydrogenation with shape-selective Pt/ZSM-5 catalysts†

J. Van Aelst,‡[a] A. Philippaerts,‡[a] E. Bartholomeeusen,[a] E. Fayad,[b] F. Thibault-Starzyk,[b] J. Lu,[c] D. Schryvers,[c] R. Ooms,[a] D. Verboekend,[a] P. Jacobs[a] and B. Sels*[a]

Pt/ZSM-5 catalysts with various crystal sizes were prepared *via* competitive ion-exchange, followed by a slow activation procedure. Even when using very large ZSM-5 crystals, highly dispersed Pt nano-clusters were contained within the zeolite crystal's voids, as ascertained by 2D pressure-jump IR spectroscopy of adsorbed CO and focussed ion-beam transmission electron microscopy. The shape-selective properties of the Pt/ZSM-5 catalysts were evaluated in the partial hydrogenation of soybean oil. Unique hydrogenation selectivities were observed, as the fatty acids located at the central position of the triacylglycerol (TAG) molecules were preferentially hydrogenated. The resulting oil has therefore high levels of intermediately melting TAGs, which are compatible with biolubricants due to their improved oxidative stability and still appropriate low-temperature fluidity. The TAG distribution in the partially hydrogenated soybean oil samples was independent from the zeolite crystal size, while the hydrogenation activity linearly increases with the crystal's external surface area. This trend was confirmed with a Pt loaded mesoporous ZSM-5 zeolite, obtained *via* a mild alkaline treatment. These observations imply and confirm a genuine pore mouth catalysis mechanism, in which only one fatty acid chain of the TAG is able to enter the micropores of ZSM-5, where the double bonds are hydrogenated by the crystal encapsulated Pt-clusters.

Introduction

ZSM-5 zeolites containing Pt particles have already proven to be valuable catalysts not only in petrochemistry,[1] but also in environmental[2] and food applications.[3] Generally, for optimal catalytic performance, the metal should be well-dispersed throughout the zeolite matrix, due to the higher available active metal surface area and the lower propensity for coke formation and catalyst deactivation. In addition, the localisation of the metal clusters in or on the zeolite crystals is especially important as it can have a major influence on the selectivity of the reaction. It is well-known that the accessibility of the interior of zeolite crystals can impose shape-selective size exclusion effects on both the feed molecules (reagent selectivity) as well as on the products that can be formed (product selectivity).[4] Therefore, active sites, *viz.* metal clusters, located inside the narrow voids of the zeolite matrix, might cause enhanced molecular shape-selectivity. Metal clusters located at the exterior surface of the zeolite crystals will not induce such size exclusion selectivity. The shape-selective hydrogenation of certain aromatics contained in a refinery gasoline or distillate pool over modified Pt/ZSM-5 catalysts, thereby reducing aromatic emissions, is a typical example of preferred intracrystalline catalysis.[5]

Next to size exclusion, molecular shape-selectivity can also arise from configurational diffusion, occurring in situations where the dimensions of the catalyst approach those of the molecules. In this diffusional regime, even a subtle change in the dimensions of a molecule can result in a large variation of its diffusivity.[4a] Though shape-selective effects are rarely described in oleochemistry,[6] it was recently shown that linear *trans* fatty acids (methyl elaidate) can be preferentially hydrogenated in the presence of the bent *cis* isomer (methyl oleate) using a shape-selective Pt/ZSM-5 catalyst.[7]

Application of the same Pt/ZSM-5 catalyst for the partial hydrogenation of model triacylglycerols (TAGs) has led to the elucidation of a new form of shape-selectivity through size exclusion. Hereby, the central fatty acid chain (often denoted as

[a] KU Leuven, Centre for Surface Chemistry and Catalysis, Leuven Chem&Tech, Celestijnenlaan 200F - box 2461, B-3001 Heverlee, Belgium.
E-mail: bert.sels@biw.kuleuven.be
[b] ENSICAEN, Université de Caen, CNRS, Laboratoire Catalyse et Spectrochimie, 6 Boulevard Maréchal Jui, 14050 Caen, France
[c] University of Antwerp, EMAT, Groenenborgerlaan 171, B-2020 Antwerpen, Belgium
† Electronic supplementary information (ESI) available. See DOI: 10.1039/c6cy00498a
‡ These authors contributed equally to this work.

2820 | *Catal. Sci. Technol.*, 2016, **6**, 2820–2828

This journal is © The Royal Society of Chemistry 2016

the *sn*-2 position) of the model TAG is preferentially reduced. This was rationalised by the hypothesis of pore mouth adsorption of TAGs in a "tuning fork" conformation, allowing the central fatty acid chain to protrude in the zeolite pores containing occluded metal (Fig. 1).[3]

Up to now, the concept of pore mouth catalysis has been used only to rationalise bifunctional catalysis of long chain *n*-alkanes with Pt-loaded zeolites, such as Pt/H-ZSM-23[8] and Pt/H-ZSM-22.[9] In this respect, pore mouth catalysis was defined as catalysis in which only a part of the molecule is physisorbed in one pore of the zeolite, the other part remaining outside. As only the pore mouths of the zeolite are active in the reaction, the use of larger zeolite crystals should not influence the shape-selective properties of the catalyst. In contrast, shape-selective properties induced by configurational diffusion would change upon increasing the crystallite size. Hereby, the increase of the imposed diffusional constraints would lead to a decreased relative conversion of the slower diffusing reagent.

In this work, the hypothesis of pore mouth catalysis over shape-selective Pt/ZSM-5 is verified by variation of the zeolite crystal size and hence the external surface area. First, a detailed microscopic and spectroscopic study is carried out to assure the intracrystalline appearance of the Pt clusters, an essential condition for pore mouth catalysis induced shape-selectivity. Additionally, also the influence of different Pt addition methods on the location and distribution of the Pt clusters will be investigated.

To compare their shape-selective properties and activity, the Pt/ZSM-5 zeolites with various crystal sizes are applied as catalysts for the partial hydrogenation of real vegetable oil, *viz.* soybean oil, containing a complex mixture of mainly poly-unsaturated TAGs. The poly-unsaturated fatty acids are preferentially present at the *sn*-2 position of the TAG molecules. TAGs are presented for example as SLO, an abbreviation based on the composing fatty acids linoleic acid (L; C18:2 *cis*-9,*cis*-12) at the central *sn*-2 position, and oleic acid (O; C18:1 *cis*-9) and stearic acid (S; C18:0) at the outer *sn*-1/3 positions. Given their excellent frictional properties, high viscosity index, low volatility and good biodegrad-

ability, vegetable oils have large potential as renewable resource for lubricants.[10] However, as a result of their high degree of poly-unsaturation, their oxidative stability and ageing resistance are rather poor. Therefore, a partial hydrogenation is necessary to reduce a substantial portion of the oxidative unstable linoleic (L) and linolenic (Ln; C18:3 *cis*-9,*cis*-12, *cis*-15) acids. Thereby, the formation of high-melting saturates (such as stearine SSS as a result of a complete and unselective hydrogenation) or *trans* isomers (as a result of double bond isomerisation) should be avoided, in order to maintain an acceptable low-temperature melting behaviour.[10] The proposed shape-selectivity of Pt/ZSM-5, *i.e.* a preferential and selective hydrogenation of linear *trans* fatty acid chains (if formed) and the saturation of fatty acids at the *sn*-2 position in the TAGs rather than those at the *sn*-1/3 positions (Fig. 1), is expected to steer the hydrogenation towards biolubricant compatible vegetable oils with an intermediate melting profile.

Results and discussion

To assess the hypothesis of pore mouth catalysis during partial hydrogenation with Pt/ZSM-5 zeolites, various ZSM-5 zeolites with different crystal sizes, but comparable Si/Al ratios, *viz.* 100–138, have been bought or synthesised. An overview of the various ZSM-5 samples is given in Table 1.

The crystals of the commercial ZSM-5 sample (CBV28014, Zeolyst; notation: Z-26) have a spherical morphology and are rather heterogeneous in size, *viz.* 0.4–2 μm (Table 1, entry 1). Home-made ZSM-5 samples Z-20, Z-2 and Z-1 were synthesised according to a published procedure (Table 1, entries 2–4).[7] Sample Z-20 also has a spherical morphology, yet the crystals are more homogeneous in size, averaged around 1 μm. Samples Z-2 and Z-1 both show a coffin-shaped morphology, having an average size of 4 × 3 × 2 μm and 11 × 7 × 5 μm, respectively. SEM images of all samples can be found in Fig. S1.†

In order to obtain a ZSM-5 sample with large external surface area, the commercial ZSM-5 sample was subjected to a mild NaOH treatment (sample Z-55; Table 1, entry 5). Such alkaline treatment creates intracrystalline mesoporosity, and thus a larger available surface area, *via* a minor dissolution of the zeolite framework.[11]

Nitrogen isotherms of the various samples reveal two hysteresis phenomena (Fig. S2†): one at low pressure ($p/p_0 = 0.1$–0.3) and one at high pressure (above $p/p_0 = 0.45$). The shape of the nitrogen isotherms is in agreement with the literature on ZSM-5 samples with a high Si/Al ratio (>50).

The sudden change in the adsorbed volume at $p/p_0 = 0.1$ is explained by a liquid-like to solid-like phase transition of adsorbed nitrogen in the channels of the near-silicalite crystals.[12] The hysteresis at high pressure is attributed to capillary condensation in the mesopores, which can be either intra- or intercrystalline. Micropore volumes and external surface areas are determined by applying the *t*-plot method on the adsorption branch of the isotherms and are compared in
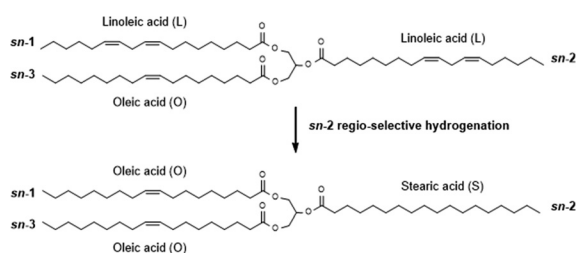

Fig. 1 Illustration of *sn*-2 regio-selective hydrogenation of triacylglycerols (TAGs) in "tuning fork" conformation. In this specific example, a LLO triacylglycerol, composed of poly-unsaturated linoleic (L) acid at positions *sn*-1 and *sn*-2 and mono-unsaturated oleic (O) acid at position *sn*-3, is partially hydrogenated to an OSO triacylglycerol. The latter is composed of a fully saturated stearic (S) acid at the central *sn*-2 position, while mono-unsaturated oleic (O) acids are present at the outer *sn*-1/3 positions.

Table 1 Physico-chemical characterisation of various ZSM-5 supports

Sample	Si/Al	Crystal size[a] [μm]	Morphology[a]	V_{tot}[b] [cm^3 g^{-1}]	V_{micro}[c] [cm^3 g^{-1}]	S_{ext}[d] [m^2 g^{-1}]
Z-26	138	0.4–2	Spherical	0.20	0.17	26
Z-20	100	0.5–1.5	Spherical	0.21	0.16	20
Z-2	110	4 × 3 × 2	Coffin	0.17	0.16	2
Z-1	115	11 × 7 × 5	Coffin	0.17	0.17	1
Z-55	—	0.2–0.3	Spherical	0.34	0.17	55

[a] Determined with SEM. [b] Determined with N_2 physisorption, adsorption value at $p/p_0 = 0.97$. [c] Determined with N_2 physisorption, derived from the positive intercept of the straight line through the t-plot data in the region from $t = 0.5$ to $t = 0.8$. [d] Determined with N_2 physisorption, derived from slope of the same straight line through the t-plot data.

Table 1. It is clear that all ZSM-5 samples have comparable total and micropore volumes. Only the Z-55 sample has a considerably higher total pore volume, which is attributed to the presence of intracrystalline mesopores. The external surface areas (S_{ext}) vary considerably, $viz.$ from 1 to 55 m^2 g^{-1}. The value of S_{ext} is used as a suffix in the notation of the various ZSM-5 samples.

Two types of Pt/ZSM-5 catalysts were prepared, using different Pt addition methods, $viz.$ incipient wetness impregnation (IWI) and competitive ion-exchange (CIE). Also a Pt/γ-alumina catalyst was prepared via IWI, and used as a reference of non-microporous material. The Pt loading (0.5 wt%) and catalyst activation procedure were equal for all samples, applying slow heating ramps in order to hinder the migration and agglomeration of Pt as described previously.[7] The most important details concerning the various Pt catalysts are summarised in Table 2.

Intra- $versus$ extracrystalline Pt clusters

From previous work using transmission electron microscopy (TEM), it is known that Pt/ZSM-5 catalysts prepared by CIE show a high Pt dispersion with small Pt nano-clusters, presumably located mainly inside the zeolite pores, whereas Pt addition with IWI leads to an asymmetric broad distribution of Pt particles, ranging from 2 to 20 nm, many of which are located outside the zeolite crystal.[7]

However, as TEM images are 2D projections of 3D objects it is not always straightforward to determine whether metal particles are located in the intracrystalline micropores or on

the external surface of the zeolite crystal. Therefore, in this work the Pt localisation on the two catalysts based on the commercial zeolite, $viz.$ Pt/Z-26-CIE and Pt/Z-26-IWI, was verified with a new technique, $viz.$ 2D pressure-jump infrared spectroscopy of adsorbed species (PJAS-IR).

The 2D PJAS-IR technique is capable of locating adsorption sites by the evolution of Fourier analysed IR spectra after a sudden change in the pressure of adsorbate in a porous material.[13] This technique allows investigating relaxation processes following this perturbation. As each adsorbed species responds with its own frequency depending on the diffusion coefficients and the adsorption energy, the location and environment can be determined.[14] Therefore 2D-PJAS-IR of adsorbed CO should reveal the location of Pt on the catalysts.

In order to assess the reliability of this method, Pt dispersions were determined via IR measurements of chemisorbed CO (see the ESI†). The quantitative response was used to determine the number of accessible Pt atoms and thus the dispersion of the Pt metal (D_{Pt}). The frequency of the IR bands also informs directly on the particle size. At room temperature, CO typically adsorbs linearly on Pt^0 clusters with characteristic IR bands in the 2100–2000 cm^{-1} range, depending on the size of the Pt clusters. A shift to lower wavenumbers of the vC–O stretching frequency of chemisorbed CO is due to smaller Pt particle size.[15] On the Pt/Z-26-CIE and Pt/Z-26-IWI samples, this peak is seen at 2075 and 2078 cm^{-1}, respectively, corresponding to linearly chemisorbed CO on the surface of small Pt^0 nanoparticles. These peaks shift to 2083 cm^{-1} with higher CO doses, due to a CO coverage effect on the Pt nanoparticles (Fig. S3†). Pt/Z-26-CIE shows a dispersion of 42% with a

Table 2 Characterisation of Pt-catalysts

Catalyst	D_{Pt}[a] [%]	Pt size[a] [nm]	D_{Pt}[b] [%]	Pt size[b] [nm]	Pt size[c] [nm]
Pt/Al$_2$O$_3$	28	2.9	—	—	—
Pt/Z-26-IWI	23	3.6	29	3.2	3–12
Pt/Z-26-CIE	40	2.0	42	2.2	1–2.5
Pt/Z-20-CIE	20	4.1	—	—	—
Pt/Z-2-CIE	11	7.5	—	—	—
Pt/Z-1-IWI	11	7.5	—	—	1–10
Pt/Z-1-CIE	15	5.5	—	—	1–3
Pt/Z-55-CIE	21	3.9	—	—	—

[a] Average based on CO-chemisorption MS measurements. [b] Average based on CO-chemisorption IR measurements. [c] Range observed by TEM measurements.

mean particle size of 2.2 nm. For Pt/Z-26-IWI, the dispersion is around 29% with a mean Pt particle size of 3.2 nm. These values are in agreement with those previously obtained from CO TPD with MS (Table 2).[7]

Next, 2D-PJAS-IR of adsorbed CO was studied on both samples to determine the Pt location. The corresponding 2D maps are presented in Fig. 2. The CIE sample (Fig. 2A) shows that the main intensity band is concentrated at high frequency (HF, 180–200 Hz) and low wavenumbers (2000–1950 cm^{-1}). The signal in the low wavenumber range is due to a reduced CO coverage on the nanoparticle surface at 300 °C. The 2D-PJAS IR map for the IWI sample (Fig. 2B) shows that the main signal is concentrated at low frequency (LF, 50–75 Hz) and around 2050–1990 cm^{-1}.

From a previous study on the sintering process of Pt on ZSM-5, it was concluded that signals at low frequency (<50 Hz) correspond to the CO adsorption–desorption oscillation process occurring on the external surface, while the signals at higher frequency (130–250 Hz) are assigned to the presence of Pt nanoclusters in the pores of ZSM-5.[14] This conclusion was rationalised by the fact that the mean free path is longer on the external surface than in the pores. Moreover, in agree-

ment with the present observations, the HF signal appearing at low wavenumbers corresponds to smaller Pt clusters compared to the LF signal appearing at higher wavenumbers.

From the 2D-PJAS-IR maps of both samples, it follows that the HF signal observed for the CIE sample can be assigned to the presence of small Pt nanoparticles within the pores of the ZSM-5 zeolite, while the LF signal observed for the IWI sample is attributed to CO adsorbed mainly on Pt nanoparticles located on the outer surface of the ZSM-5 crystals. Thus, when Pt is added to ZSM-5 *via* competitive ion-exchange and subsequently activated *via* calcination and reduction methods, applying slow heating rates, it is feasible to obtain shape-selective Pt/ZSM-5 catalysts with all Pt located inside the zeolite pores.

In contrast to the commercial ZSM-5 catalysts, the Pt distribution and localisation in large ZSM-5 crystals have not been studied before and therefore were assessed in this work prior to evaluating their catalytic hydrogenation properties, using focussed ion-beam transmission electron microscopy (FIB-TEM). FIB-TEM is a highly valuable technique for determining the distribution of Pt clusters throughout the zeolite crystal. Using this technique, thin sections of the zeolite crystal can be prepared by FIB milling and are then visualised in TEM. As this technique is especially valuable for determining the metal distribution in large crystals, Pt/Z-1-IWI and Pt/Z-1-CIE catalysts with dimensions of about 11 × 7 × 5 μm, were selected for characterisation with FIB-TEM. From both samples, a FIB lamella was taken in the middle of the zeolite crystal (Fig. 3; left). Due to the twinned nature of the coffin-shaped zeolites, intergrowths and cracks in the lamella are clearly visible with SEM (Fig. 3; right), in agreement with previous studies.[16]

Conventional bright field (BF) TEM images of the FIB lamella of the impregnated sample are shown in Fig. 4a. In these images, the strongly diffracting and absorbing Pt clusters show up as black dots. It is clear that the Pt clusters are not homogeneously distributed and are mainly located in and near the cracks. This inhomogeneous distribution of Pt particles can also be noted in the STEM images, in which the Z-contrast of the incoherent scattering reveals the Pt clusters as white particles, as seen in Fig. 4b. Most Pt clusters have sizes around 1–3 nm, although also Pt clusters larger than 5 nm can be observed, suggesting a bimodal distribution.
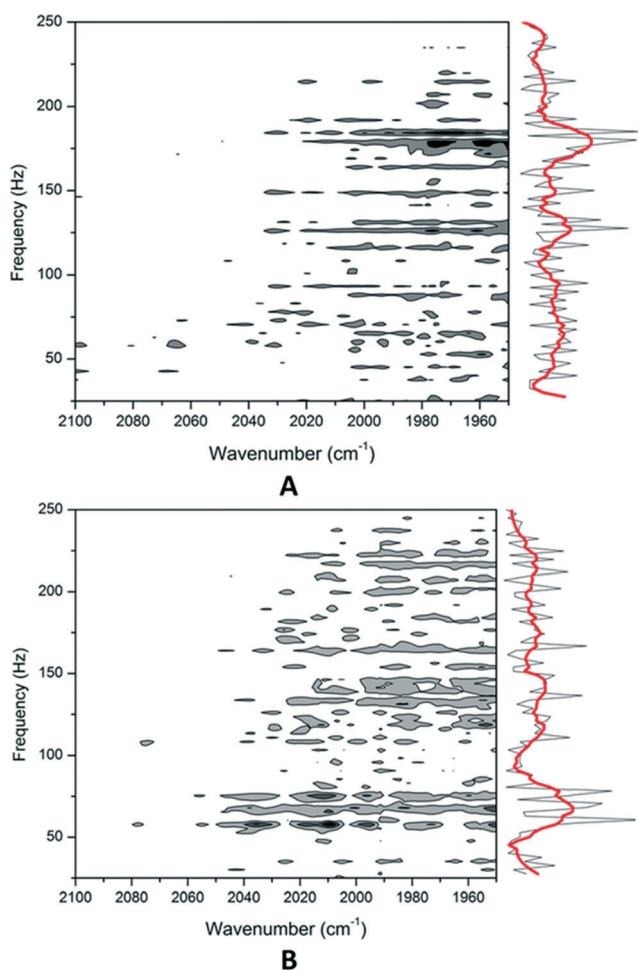

Fig. 2 2D PJAS-IR maps (at 300 °C) of CO adsorbed on Pt/ZSM-5: (A) Pt/Z-26-CIE and (B) Pt/Z-26-IWI.
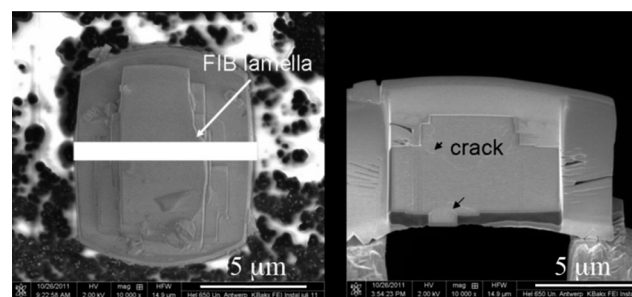

Fig. 3 SEM images of (left) the large coffin-shaped Z-1 ZSM-5 crystal and (right) the FIB lamella.

This journal is © The Royal Society of Chemistry 2016

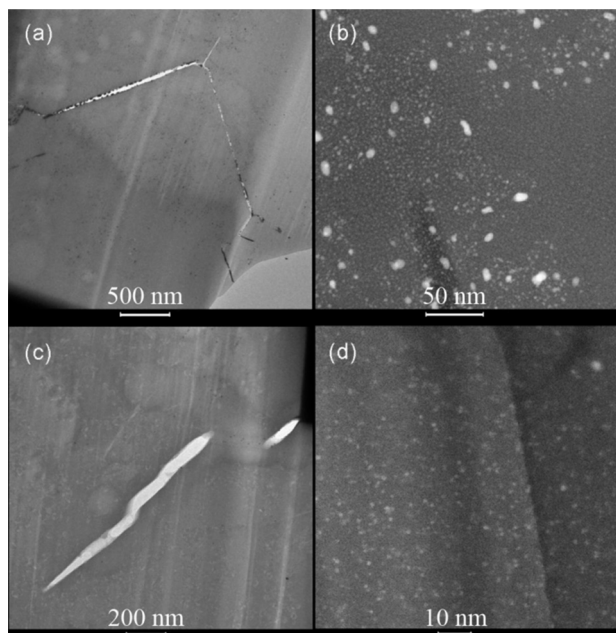*Catal. Sci. Technol.*, 2016, **6**, 2820–2828 | **2823**

Fig. 4 FIB-(S)TEM images of the Pt/Z-1-IWI sample, (a) showing Pt particles as dark spots agglomerated at interfaces and (b) the inhomogeneous distribution of small and large Pt particles as bright spots; and of the Pt/Z-1-CIE sample, (c) showing a few Pt particles as dark spots and (d) homogeneously distributed small Pt particles as bright spots.

Compared to the IWI-sample, the Pt clusters are smaller and much more homogeneously distributed in the CIE-sample. TEM images at different spots of the FIB lamella show the presence of small Pt clusters throughout the sample (confirmed by EDX). These highly dispersed Pt nano-clusters are more clearly visible in STEM images (Fig. 4d). The Pt clusters in this sample are all very small, viz. around 1–2 nm, with only few larger particles seen in Fig. 4c obtained from the top-right part of the lamella. The bright bubble-like features in this image are due to starting radiation damage.[16d]

From FIB-TEM measurements it can thus be concluded that it is feasible to obtain shape-selective Pt/ZSM-5 catalysts, in which the Pt-nanoclusters are homogeneously distributed throughout the zeolite crystal, even when very large ZSM-5 crystals are used, provided that the Pt addition occurs via a competitive ion-exchange, followed by careful calcination and reduction procedures.

Selective partial hydrogenation

Partial hydrogenation of vegetable oils is an important process in oleochemistry, and historically also strongly associated with food processing.[17] The aim of this reaction is to selectively hydrogenate air-unstable polyunsaturated fatty acids, like linolenic (Ln) and linoleic (L) acid, to the more stable mono-unsaturated oleic (O) acid. For use of partially hydrogenated oils as stable biolubricant, the formation of trans isomers or fully saturated stearic (S) acids should be minimised,

as their high melting points lead to adverse physical properties.[10]

Earlier work with shape-selective Pt/ZSM-5 has proven the occurrence of such preferential stepwise reduction of unsaturates without significant cis/trans isomerisation during hydrogenation of complex mixtures of TAGs present in real edible oils.[17a] In addition, high percentages of intermediately melting TAGs were observed, resulting from an increased selectivity for hydrogenation of the fatty acids located at the central (sn-2) position (Fig. 1). This sn-2 regio-selectivity can be explained by pore mouth catalysis, in which one fatty acid chain is adsorbed in the pore where it reacts with intrapore Pt clusters, whereas the other two fatty acid chains, located at sn-1 and sn-3 in the TAGs, largely remain outside and will not react.[3]

To confirm this pore mouth mechanism, the different Pt/ZSM-5 zeolites with various crystal sizes and hence external surface areas (S_{ext}), all with homogeneously distributed intracrystalline Pt clusters prepared via CIE, are applied as catalysts for the partial hydrogenation of soybean oil. The results from the FIB-TEM study assure that influences on the hydrogenation performance cannot be caused by differences in Pt location or distribution.

The initial activity and the selectivity towards intermediately melting TAGs at a conversion of 30% are plotted as functions of S_{ext} in Fig. 5. It is clear that the external surface area has a significant impact on the catalytic activity. The initial activity decreases from 2.33 mol of double bonds converted per minute per g of available Pt for the commercial
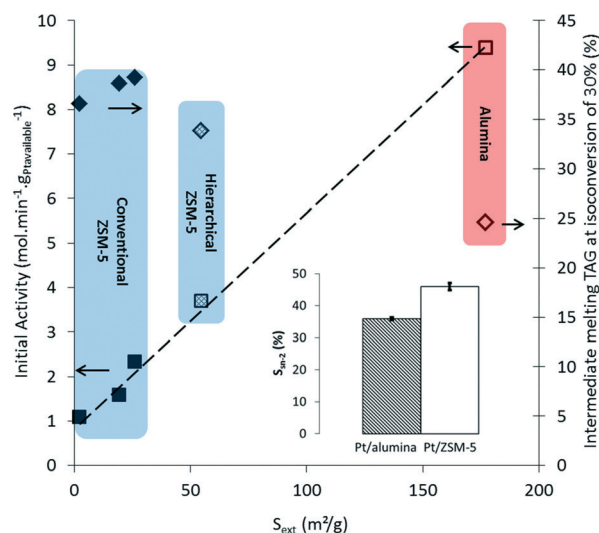

Fig. 5 Influence of S_{ext} (S_{total} in the case of the alumina support) of the various Pt catalysts on the initial activity (calculated as mol min^{-1} (g_{Pt} D_{Pt})$^{-1}$) and the hydrogenation selectivity, here expressed as the level of intermediately melting TAGs at 30% conversion (IV = 90) and the selectivity S_{sn-2} for the hydrogenation of the fatty acids located at the central sn-2 position, calculated as the conversion on sn-2/ (conversion on sn-2 + conversion on sn-1/3). 100%, at a total conversion of ±25 mol% (IV = 100). All Pt/ZSM-5 catalysts are prepared via competitive ion exchange, whereas Pt/alumina is prepared via incipient wetness impregnation.

2824 | Catal. Sci. Technol., 2016, **6**, 2820–2828

This journal is © The Royal Society of Chemistry 2016

based Pt/Z-26-CIE sample with an external surface area of 26 m^2 g^{-1}, to a value of 1.09 for the large coffin-shaped crystals of the Pt/Z-2-CIE catalyst with an external surface area of 2 m^2 g^{-1}. Note that the hydrogenation results of the catalyst Z-1-CIE are not plotted in Fig. 5. Due to the extremely low activity of this catalyst, it was not possible to obtain a conversion of 30%. A value for the catalytic activity as high as 9.39 mol min^{-1} $g_{Ptavailable}^{-1}$ is obtained with Pt/alumina with a total surface area of 177 m^2 g^{-1}. Fig. 5 clearly shows a linear increase of the initial activity with increasing S_{ext}. This trend was further corroborated by evaluating the Pt-loaded mesoporous ZSM-5 catalyst in the hydrogenation of soybean oil. Increasing the external surface of the commercial catalyst from 26 to 55 cm^3 g^{-1}, *via* a NaOH treatment, leads to an increase in the initial activity from 2.33 to 3.71 mol min^{-1} $g_{Ptavailable}^{-1}$.

Despite the major influence on the activity, the selectivity of the reaction is hardly affected when using shape-selective Pt loaded ZSM-5 zeolites with varying crystal sizes. At the same conversion, nearly the same TAG compositions are obtained in the resulting partially hydrogenated samples (see Fig. 6). Note the substantial shift in composition from the original soybean TAGs towards triglycerides with less unsaturated bonds, as reflected by the higher equivalent carbon number (ECN; see Table S1†). Meanwhile, the undesired full hydrogenation towards (too high melting) saturates (with ECN of 52 like SSO and 54 like SSS) is very limited, in contrast to the result with the Pt/alumina catalyst. It is apparent from Fig. 5 that the selectivity towards intermediately melting triglycerides (ECN of 48 like OOO and 50 like SOO) is similar for all Pt/ZSM-5 samples, *viz.* 36.6–39.2% at IV = 90, and significantly higher compared to the level obtained with Pt/alumina, *viz.* 24.6% at a total conversion of 30%. In addition,
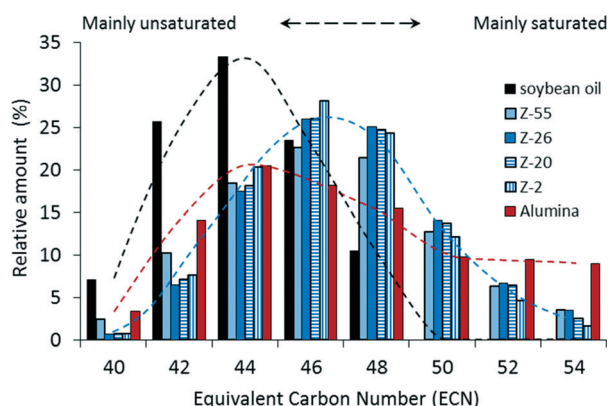
also the hydrogenation selectivity of the fatty acids located at the *sn*-2 position (S_{sn-2}) is comparable for the various shape-selective Pt/ZSM-5 catalysts and significantly higher compared to the Pt/alumina catalyst. These shape-selective features, determined by the location of the Pt clusters within the pores of ZSM-5, are thus independent of the zeolite crystal size. This implies and confirms that the hydrogenation of soybean oil on shape-selective Pt/ZSM-5 proceeds *via* pore mouth catalysis.

Importantly, also increasing the external surface area *via* a mild NaOH treatment, hardly influences the selectivity in the hydrogenation of soybean oil (Fig. 5 and 6), suggesting that also in hierarchical ZSM-5 (Z-55) the Pt clusters are located mainly in the micropores. Taking the higher activity and comparable selectivity into account, hierarchisation of commercially available zeolites thus appears to result in promising catalysts for active and selective partial hydrogenation of vegetable oils.

Conclusions

Shape-selective Pt/ZSM-5 catalysts, with all Pt located in the intracrystalline voids for a loading of 0.5 wt%, can be synthesised by competitive ion-exchange, followed by a slow temperature-activation procedure. The intracrystalline location of the Pt nano-clusters is confirmed by using 2D pressure-jump IR spectroscopy of adsorbed CO. Moreover, FIB-TEM indicates that even in large ZSM-5 crystals, Pt-nano-clusters are homogeneously distributed throughout the zeolite crystals. To achieve this, it is crucial to add the Pt metal complex *via* competitive ion-exchange. Shape-selective properties, determined by the location of the Pt clusters within the small pores of ZSM-5, are confirmed in the partial hydrogenation of soybean oil. The resulting high hydrogenation selectivity towards intermediately melting TAGs, attributed to a distinct *sn*-2 regio-selectivity and essentially precluding complete saturation of TAG molecules, and the independence of this selectivity to the zeolite crystal size, are the most important characteristics to address that hydrogenation of TAGs on shape-selective Pt/ZSM-5 proceeds *via* pore mouth catalysis. Due to the improved oxidative stability and appropriate low-temperature fluidity, the partially Pt/ZSM-5 hydrogenated vegetable oil is promising as a renewable feedstock for biolubricants.

Fig. 6 Triacylglycerol composition according to their equivalent carbon number (ECN) of the starting soybean oil (in black) and the fat mixtures (at IV = 90) hydrogenated by different Pt catalysts. All Pt/ZSM-5 catalysts (in blue) are prepared *via* competitive ion-exchange, whereas Pt/alumina (in red) is prepared *via* incipient wetness impregnation. Lines connect the relative amount of each TAG family with certain ECN and therefore show the (shift in) TAG distribution before (black) and after partial hydrogenation in the presence of shape-selective (blue, intermediately melting fatty product) and non-selective (red, highly melting fatty product) catalysts.

Experimental

Soybean oil was kindly provided by Oleon (Belgium). NH_4-ZSM-5 zeolite powder (CBV28014, Si/Al = 138) is from Zeolyst. γ-Alumina was purchased from Aldrich (Type 507C). Synthesis of ZSM-5 zeolites was according to a previously described procedure with colloidal SiO_2 (LUDOX®AS-40, 40 wt% suspension in water) as Si-source, $Al(NO_3)_3 \cdot 9H_2O$ as Al-source, tetrapropylammonium (TPA) bromide as templating agent and 1-hexanol/water mixtures as solvent.[7] Alkaline treatment was performed by addition of the zeolite (33 g L^{-1}) to a

This journal is © The Royal Society of Chemistry 2016

Catal. Sci. Technol., 2016, **6**, 2820–2828 | **2825**

vigorously-stirred aqueous solution of 0.15 M NaOH at 65 °C for 30 min. The reaction was followed by quenching, filtration, extensive washing using distilled water, and overnight drying at 80 °C. Pt catalysts were synthesised as described previously.[7]

Platinum dispersions were determined using CO chemisorption MS. Catalyst pellets loaded in a tubular reactor were reduced according to the above described pretreatment procedures and cooled down to room temperature under flowing He. For the titration of the Pt surface, pulses of 5 µL of pure CO were added to a He flow of 10 mL min^{-1} at an interval of 2 min. The CO concentration in the outlet stream was followed continuously *via* ion monitoring at m/z = 28 with a Pfeiffer Omnistar quadrupole mass spectrometer. For the calculation of the dispersion, adsorption of 1 CO per accessible Pt atom was assumed. The size of Pt particles, d_{Pt}, was derived from the Pt dispersion, D_{Pt}, assuming a cubic particle shape.[18]

$$d_{Pt} = 0.821\left(\frac{1}{D_{Pt}}\right)$$

CO chemisorption IR experiments were performed under vacuum in a quartz IR cell equipped with KBr window. The IR experiments were performed on a Bruker IFS 66 FTIR instrument equipped with a cryogenic MCT detector and running at 8 cm^{-1} resolution. The catalyst powder was pressed and used as wafers of 20 mg (10 mg cm^{-2}). Samples were activated at 673 K under an oxygen atmosphere (~100 Torr) in order to remove impurities. A static reduction under H$_2$ (~100 Torr) at 673 K followed by evacuation was then repeated twice. Small calibrated doses of CO were sent afterwards at RT on the activated sample leading to an increase of the ν_{CO} IR bands of CO chemisorbed on the Pt surface atoms.

Two Dimensional Pressure Jump of the Adsorbed Species IR studies (2D-PJAS-IR) consist of the variation of the IR cell volume inducing a pressure jump of the CO adsorbed species on the zeolite system and monitored by IR spectroscopy. This recent technique already described elsewhere[13] allows investigating relaxation processes occurring at the end of the perturbation. As each adsorbed species responds with its own frequency depending on the diffusion coefficients and the adsorption energy, the location and environment could be determined. The sample treatment and activation procedure were the same as for the CO chemisorption. A mixture of CO/He (1/10; 33 Torr) was introduced at RT followed by heating up to 573 K. Afterwards, the 2D-PJAS experiment was performed on Pt/ZSM-5 with 5 co-additions and the IR spectra were recorded in the step scan mode.[19] CO adsorption for the 2D-PJ experiment was performed at an unusually high temperature in order for the adsorption equilibrium to be easily shifted by the pressure swing.[14] The fairly high pressure (compared to usual *in situ* infrared experiments) increases the amount of CO adsorbed on the metal above the detection limit of an MCT detector.

Cross-section FIB lamellas were prepared with the so-called "lift out" technique using an FEI Helios NanoLab 650 FIB/SEM dual-beam system. An ion-beam-assisted (30 kV) protective Pt layer was deposited on the surface of the crystal before FIB cutting. Ga$^+$ ion beams of 30 kV/2.5 nA and 30 kV/0.23 nA were used for sample cutting and early stage milling, respectively. In the final stage, the Ga$^+$ beam was reduced to 5 kV/14 pA to minimise the ion beam damage during final milling. Conventional TEM and HAADF-STEM observations were performed on an FEI Tecnai microscope operated at 80–200 kV. Since the Pt-ZSM-5 samples are very sensitive to the electron beam, the samples were entered in the TEM vacuum at least 6 hours before the observations in order to allow maximum evaporation of any residual water molecules.

Hydrogenation of soybean oil was carried out in a 100 mL Parr-autoclave with sampling device. Hydrogenation reactions were conducted at 65 °C and 60 bar H$_2$ pressure under constant stirring (500 rpm). In a typical experiment, 40 g of soybean oil and an amount of catalyst at a concentration of 1–5 wt% (g$_{catalyst}$ g$_{oil}^{-1}$) were loaded in the reactor.

Triacylglycerol (TAG) composition was determined by reversed-phase high performance liquid chromatography (RP-HPLC), using a Supelcosil TM LC-18 column (25 cm × 4.6 mm; 5 µm). The column temperature was kept at 40 °C. The mobile phase was a mixture of 70% (v/v) methanol and 30% (v/v) chloroform, and was used at a rate of 1.5 mL min^{-1}. 10 µL samples prepared at 0.07 g mL^{-1} concentration with chloroform as the solvent were injected. Quantification of triacylglycerols was based on relative peak areas. Identification of triacylglycerols was carried out by comparison of retention time and equivalent carbon number (ECN) based on commercial standards. The compounds are separated by the chain length of their fatty acids as well as by their degree of unsaturation. Each double bond reduces the retention by the equivalent of two carbon atoms. This is reflected in the ECN, which is defined as CN − 2n, in which CN is the sum of the carbon atoms in the fatty acid residues of a TAG molecule, and n the number of double bonds. Triacylglycerol molecules with identical ECN will co-elute.

The fatty acid composition of the samples was determined by analyzing the corresponding fatty acid methyl esters (FAME) by gas chromatography. The triglycerides are first converted to FAME by methanolysis. In this reaction, a sample of 300 µL is dissolved in 3 mL of diethylether and reacted with a solution of 3 mL of 5% KOH in methanol. After 15 min the transesterification reaction is stopped through addition of 3 mL of octane. The formed methyl esters migrate to the octane phase, which is subsequently washed three times with 3 mL of distilled water in order to remove glycerol and K$^+$ soaps. The FAMEs were analyzed by using a Hewlett Packard HP 6890 gas chromatograph with a split injection system (split ratio = 100 : 1) and N$_2$ as the carrier gas. A 100 m CP-SIL-88 highly polar capillary column with an internal diameter of 0.25 mm and a film thickness of 0.2 µm is used for separation. Initially, the column temperature is kept at 180 °C for 50 min, and then raised at 10 °C min^{-1} to 225 °C

2826 | *Catal. Sci. Technol.*, 2016, **6**, 2820–2828

This journal is © The Royal Society of Chemistry 2016

and held for 15 min. The FID used was kept at 280 °C. Heptadecane was used as an external standard for quantification. FAMEs were identified based on retention times, using a FAME MIX C14-C22 reference from Supelco.

The degree of hydrogenation was also monitored by determining the iodine value (IV) of the products. Iodine values (g of iodine necessary for complexation with the double bonds present in 100 g of fat substrate) were calculated from the GC composition.

Regio-specific analysis of triglyceride molecules is carried out using a sn-1,3 specific pancreatic lipase (Sigma Aldrich) according to the procedure of Luddy et al., 1964.[20] The sn-2-mono-acylglycerols are separated by means of TLC with chloroform/acetone/formic acid (85/15/1) as the mobile phase. 20 dots of 40 μL were separated; the mono-acylglycerol fraction was scraped off, dissolved in diethyl-ether, converted to FAMEs by means of a methanolysis step and analyzed by GC. The fatty acid composition of the sn-1,3-positions was calculated from the concentrations in the intact triglyceride (TG) and in sn-2-mono-acylglycerol (MG) with the following equation: TG = 2/3 × sn-1,3 + 1/3 × sn-2-MG.

The selectivity for the hydrogenation of fatty acids located at the central (sn-2) position was calculated according to the formula given in the equation below.

$$S_{sn-2} = \frac{X_{sn-2}}{X_{sn-2} + X_{sn-1/3}} \cdot 100$$

in which X_{sn-2} and X_{sn-3} denote the (hydrogenation) conversion of the double bonds of fatty acids located at the sn-2 and sn-1/3 positions, respectively.

Acknowledgements

References

1 (a) N. Y. Chen and D. E. Walsh, US 4808296, 1989; (b) L. R. R. de Araujo and M. Schmal, Appl. Catal., A, 2000, 203, 275.

2 Y. Yamasaki, M. Matsuoka and M. Anpo, Catal. Lett., 2003, 91, 111.

3 A. Philippaerts, S. Paulussen, A. Beersch, S. Turner, O. I. Lebedev, G. Van Tendeloo, B. Sels and P. Jacobs, Angew. Chem., Int. Ed., 2011, 50, 3947.

4 (a) N. Y. Chen, W. E. Garwood and F. G. Dwyer, Shape selective catalysis in industrial applications, Marcel Dekker, Inc., New York, 2nd edn, 1996; (b) P. B. Weisz, Pure Appl.

Chem., 1980, 52, 2091; (c) S. M. Csicsery, Pure Appl. Chem., 1986, 58, 841.

5 R. M. Dessau, US 5350504, 1994.

6 T. Ennaert, J. Van Aelst, J. Dijkmans, R. De Clercq, W. Schutyser, M. Dusselier, D. Verboekend and B. F. Sels, Chem. Soc. Rev., 2016, 45, 584.

7 A. Philippaerts, S. Paulussen, S. Turner, O. I. Lebedev, G. Van Tendeloo, H. Poelman, M. Bulut, F. De Clippel, P. Smeets, B. Sels and P. Jacobs, J. Catal., 2010, 270, 172.

8 W. Huybrechts, G. Vanbutsele, K. J. Houthoofd, F. Bertinchamps, C. S. Laxmi Narasimhan, E. M. Gaigneaux, J. W. Thybaut, G. B. Marin, J. F. M. Denayer, G. V. Baron, P. A. Jacobs and J. A. Martens, Catal. Lett., 2005, 100, 235.

9 J. A. Muñoz Arroyo, G. G. Martens, G. F. Froment, G. B. Marin, P. A. Jacobs and J. A. Martens, Appl. Catal., A, 2000, 192, 9.

10 (a) J. C. J. Bart, E. Gucciardi and S. Cavallaro, Biolubricants Science and technology, Woodhead Publishing Limited, Cambridge, 2013; (b) H. Wagner, R. Luther and T. Mang, Appl. Catal., A, 2001, 221, 429; (c) S. Soni and M. Agarwal, Green Chem. Lett. Rev., 2014, 7, 359; (d) B. Shomchoam and B. Yoosuk, Ind. Crops Prod., 2014, 62, 395; (e) A. F. Trasarti, D. J. Segobia, C. R. Apesteguıa, F. Santoro, F. Zaccheria and N. Ravasio, J. Am. Oil Chem. Soc., 2012, 89, 2245; (f) B. Nohaira, C. Especela, G. Lafayea, P. Marecot, L. C. Hoang and J. Barbiera, J. Mol. Catal. A: Chem., 2005, 229, 117; (g) N. Ravasio, F. Zaccheria, M. Cargano, S. Recchia, A. Fusi, N. Poli and R. Psaro, Appl. Catal., A, 2002, 233, 1.

11 D. Verboekend, S. Mitchell, M. Milina, J. C. Groen and J. Pérez-Ramírez, J. Phys. Chem. C, 2011, 115, 14193.

12 (a) P. Voogd, J. J. F. Scholten and H. van Bekkum, Colloids Surf., 1991, 55, 163; (b) P. Hudec, A. Smieskova, Z. Zidek, P. Schneider and O. Solcova, Stud. Surf. Sci. Catal., 2002, 142, 1587.

13 S. Chenevarin and F. Thibault-Starzyk, Angew. Chem., Int. Ed., 2004, 43, 1155.

14 M. Rivallan, E. Seguin, S. Thomas, M. Lepage, N. Takagi, H. Hirata and F. Thibault-Starzyk, Angew. Chem., Int. Ed., 2010, 49, 785.

15 R. M. Rioux, J. D. Hoefelmeyer, M. Grass, H. Song, K. Niesz, P. Yang and G. A. Somorjai, Langmuir, 2008, 24, 198.

16 (a) M. B. J. Roeffaers, G. De Cremer, J. Libeert, R. Ameloot, P. Dedecker, A.-J. Bons, M. Bückins, J. A. Martens, B. F. Sels, D. E. De Vos and J. Hofkens, Angew. Chem., 2009, 121, 9449; (b) M. B. J. Roeffaers, R. Ameloot, M. Baruah, H. Uji-i, M. Bulut, G. De Cremer, U. Müller, P. A. Jacobs, J. Hofkens, B. F. Sels and D. E. De Vos, J. Am. Chem. Soc., 2008, 130, 5763; (c) L. Karwacki, M. H. F. Kox, D. A. M. de Winter, M. R. Drury, J. D. Meeldijk, E. Stavitski, W. Schmidt, M. Mertens, P. Cubillas, N. John, A. Chan, N. Kahn, S. R. Bare, M. Anderson, J. Kornatowski and B. M. Weckhuysen, Nat. Mater., 2009, 8, 959; (d) J. Lu, M. B. J. Roeffaers, E. Bartholomeeusen, B. F. Sels and D. Schryvers, Microsc. Microanal., 2014, 20, 42.

17 (a) A. Philippaerts, A. Breesch, G. De Cremer, P. Kayaert, J. Hofkens, G. Van den Mooter, P. Jacobs and B. Sels, J. Am.

This journal is © The Royal Society of Chemistry 2016

Catal. Sci. Technol., 2016, 6, 2820–2828 | 2827

Oil Chem. Soc., 2011, **88**, 2023; (*b*) A. Philippaerts, P. Jacobs and B. Sels, *Angew. Chem., Int. Ed.*, 2013, **52**, 5220.

18 M. G. White, *Heterogeneous Catalysis*, Prentice Hall, Englewood Cliffs, NJ, 1991.

19 T. J. Johnson, A. Simon, J. M. Weil and G. W. Harris, *Appl. Spectrosc.*, 1993, **47**, 1376.

20 F. E. Luddy, P. Magidman, S. F. Herb, R. W. Riemenschneider and R. A. Barford, *J. Am. Oil Chem. Soc.*, 1964, **41**, 693.